Journal of Peptide Science
J. Peptide Sci. **11**: 617–626 (2005)
Published online 17 May 2005 in Wiley InterScience (www.interscience.wiley.com). DOI: 10.1002/psc.677

JOURNAL OF PEPTIDE SCIENCE

$G\alpha_s$ protein C-terminal α-helix at the interface: does the plasma membrane play a critical role in the $G\alpha_s$ protein functionality?

STEFANIA ALBRIZIO,[a] GABRIELLA CALIENDO,[b] GERARDINO D'ERRICO,[c] ETTORE NOVELLINO,[a] PAOLO ROVERO[d] and ANNA MARIA D'URSI[b]*

[a] Dipartimento di Chimica Farmaceutica e Tossicologica, Università di Napoli ''Federico II'', 80131 Napoli, Italy
[b] Dipartimento di Scienze Farmaceutiche, Università di Salerno, 84084 Salerno, Italy
[c] Dipartimento di Chimica, Università di Napoli 'Federico II', 80126 Napoli, Italy
[d] Laboratorio di Chimica e Biologia di Peptidi e Proteine, Dipartimento di Scienze Farmaceutiche, Università di Firenze, 50019 Sesto Fiorentino, Italy

Received 12 January 2005; Accepted 4 March 2005

Abstract: The heterotrimeric guanine nucleotide-binding regulatory proteins (G proteins, $G\alpha\beta\gamma$) mediate the signalling process of a large number of receptors, known as G protein-coupled receptors. The *C*-terminal domain of the heterotrimeric G protein α-subunit plays a key role in the selective activation of G proteins by their cognate receptors. The interaction of this domain can take place at the end of a cascade including several successive conformational modifications. $G\alpha_s(350–394)$ is the 45-mer peptide corresponding to the *C*-terminal region of the $G\alpha_s$ subunit. In the crystal structure of the $G\alpha_s$ subunit it encompasses the $\alpha4/\beta6$ loop, the $\beta6$ β-sheet segment and the $\alpha5$ helix region. Following a previous study based on the synthesis, biological activity and conformational analysis of shorter peptides belonging to the same $G\alpha_s$ region, $G\alpha_s(350–394)$ was synthesized and investigated. The present study outlines the central role played by the residues involved in the $\alpha4/\beta6$ loop and $\beta6/\alpha5$ loops in the stabilization of the *C*-terminal $G\alpha_s\alpha$-helix. $H_2O/^2H_2O$ exchange experiments, and NMR diffusion experiments show interesting evidence concerning the interaction between the SDS micelles and the polypeptide. These data prompt intriguing speculations on the role of the intracellular environment/cellular membrane interface in the stabilization and functionality of the *C*-terminal $G\alpha_s$ region. Copyright © 2005 European Peptide Society and John Wiley & Sons, Ltd.

Keywords: conformation; $G\alpha_s$ peptides; α-helix; NMR; SDS micelles; 3D-structure

INTRODUCTION

The heterotrimeric guanine nucleotide-binding regulatory proteins (G proteins, $G\alpha\beta\gamma$) mediate the signalling process of a large number of receptors, known as GPCRs, thus controlling essential functions in all tissues and throughout all eukaryote species [1]. Their involvement in several diseases have made GPCRs important molecular targets for the development of new drugs.

Much effort has been spent to obtain a complete understanding of the molecular basis of the G protein/receptor interaction. If the plethora of biochemical data support the key role of the $G\alpha$ *C*-terminus in the G protein/receptor interaction, the centrality of this region in the coupling with its cognate receptor is not straightly and clearly supported by structural evidence. Crystal structures of $G\alpha_t$, $G\alpha_i$ and $G\alpha_s$ [2–6] show that the *C*-terminal region of $G\alpha$ subunits is arranged in an α-helical structure. However, the last three ($G\alpha_s$) to eight ($G\alpha_i$ and $G\alpha_t$) residues are unordered in these structures. NMR studies [7] of a $G\alpha_t$ *C*-terminal undecapeptide, $G\alpha_t(340–350)K341R$, have shown that the conformation of the last residues is unordered in the presence of dark rhodopsin while they form a β-turn when bound to the photoisomerized rhodopsin, metarhodopsin II. On the other hand, a more recent NMR investigation [8] indicates that in the presence of photoisomerized rhodopsin the $G\alpha_t$ *C*-terminal undecapeptide forms a continuous α-helix including helix $\alpha5$ of the protein. Recently, experiments of residue dipolar couplings led to the determination of the position of an

Abbreviations: Abbreviations: CD, circular dichroism; DPC, dodecyl phosphocholine; DPPC, dipalmitoyl phosphatidylcholine; DQF-COSY, double quantum filtered correlated spectroscopy; ESI-MS, electron spray mass spectroscopy; Fmoc, 9-fluorenylmethoxycarbonyl; $G\alpha$ and $G\beta\gamma$, the α and $\beta\gamma$ subunits of heterotrimeric G proteins; G_s, a G protein linked with the activation of adenylyl cyclase; $G\alpha_s$, the α subunit of G_s; G_i, a G protein linked with the inhibition of adenylyl cyclase; $G\alpha_i$, the α subunit of G_i; G_t (or transducin), the G protein present in rod outer segments; $G\alpha_t$, the α subunit of G_t; $G\alpha_s(374–394)C379A$, a synthetic peptide corresponding to those residues of $G\alpha_s$ with a cysteine substituted by an alanine (a $G\alpha$ subunit followed by numbers refers to the corresponding peptide); GPCR, G-protein coupled receptor; $GTP\gamma S$, guanosine-5′-O-(3-thiotriphosphate); MD, molecular dynamics; NOE, nuclear Overhauser effect; NOESY, nuclear Overhauser enhancement spectroscopy; PFG NMR; pulsed-field gradient NMR; Pmc, 2,2,5,7,8-pentamethylchroman-6-sulfonyl; SDS, sodium dodecylsulphate; tBu, t-butyl; TFA, trifluoroacetic acid; TOCSY, total correlated spectroscopy; Trt, trityl.

*Correspondence to: A. M. D'ursi, Dipartimento di Scienze Farmaceutiche, Università di Salerno, Via Ponte Don Melillo 11C, 84084 Salerno, Italy; e-mail: dursi@unisa.it

analogue of the $G\alpha_t$ subunit *C*-terminal undecapeptide relative to the membrane receptor rhodopsin. The axis of the helix exhibited by the undecapeptide makes an angle of 40° (±4°) with the membrane [9].

Previous work reported the synthesis, biological activity and conformational data of a series of peptide segments (from 11 to 21 residues) derived from the *C*-terminal sequence of the $G\alpha_s$ protein coupled with the A_{2A} adenosine receptor. The results clearly demonstrated a correlation between the biological activity of the *C*-terminal segments and the size of the peptides. An NMR investigation showed that, consistent with the crystal structure, the segments are characterized by an α-helical arrangement in the *C*-terminal region, the extent of which depends on the size of the peptide [10–12].

Many biological data point out that *C*-terminus G protein/GPCR interaction is the last step of several successive conformational modifications in which the region including the $\alpha4/\beta6$ loop and the $\beta6$ sheet plays a central role in the activation of the receptor. Accordingly, the *C*-terminus might function only as a G protein/GPCR docking site, whereas the conformational change that causes activation of the $G\alpha$ protein occurs after interaction of the receptor with another binding site of the $G\alpha$ protein, the $\alpha4/\beta6$ loop [13–16].

$G\alpha_s(350–394)$ is a synthetic polypeptide corresponding to the region of the $G\alpha_s$ subunit that, in the crystal structure of the native protein, encompasses the $\alpha4/\beta6$ loop, the $\beta6$ sheet and the $\alpha5$ helix region [6]. Following our previous studies on 21, 15 and 11-mer $G\alpha_s$ *C*-terminal peptides, an NMR structural investigation of $G\alpha_s(350–394)$ was performed in an attempt to understand the contribution of additional residues to the structural arrangement of the *C*-terminal α-helix and to shade light on the role of the $\alpha4/\beta6$ loop in the G protein/GPCRs coupling.

The interaction between the G protein and GPCR takes place in an environment characterized by physico-chemical properties very similar to those of many hormones interacting with membrane receptors. For these mediators structural investigations in membrane mimicking environments, such as micellar solutions of SDS, DPC and DPPC, are very common [17].

To evaluate the contribution of the membrane environment to the structural arrangement of $G\alpha_s(350–394)$, NMR studies were performed in a membrane mimicking environment made up of a SDS micellar solution.

Our study outlined the central role played by the residues encompassing the $\alpha4/\beta6$ and $\beta6/\alpha5$ loops in the stabilization of the $G\alpha_s$ *C*-terminal α-helix. Interestingly, the data relative to the interaction between the SDS micelles and the polypeptide stimulate speculation concerning the physico-chemical basis of the stability and the functionality of $G\alpha_s$ *C*-terminal portion.

MATERIALS AND METHODS

Peptide Synthesis

The peptide $G\alpha_s(350–394)$ was synthesized manually by the solid-phase method using Fmoc/tBu chemistry, as previously described [18]. For the N^{α}-Fmoc-protected amino acids, the following side-chain protecting groups were used: Arg(Pmc); Asn(Trt); Asp(*t*Bu); Gln(Trt), Glu(*t*Bu); His(Trt); Ser(*t*Bu); Thr(*t*Bu) and Tyr(*t*Bu). The crude peptide was purified to homogeneity by reverse-phase semi-preparative HPLC on a Vydac C18 column (2.2 × 25 cm) using a linear gradient starting from 20% CH_3CN (0.15%/min) in water containing 0.1% TFA, at a flow rate of 4 ml/min. UV detection: 210 nm. The final product was obtained by lyophilization of the appropriate fractions after removal of the CH_3CN by rotatory evaporation. Analytical HPLC was performed on a Vydac C18 column (250 × 4.6 mm) using a linear gradient starting from 20% CH_3CN (3%/min) in water containing 0.1% TFA, at a flow rate of 1 ml/min, UV detection: 210 nm. The product had a retention time of 10.6 min and showed an HPLC purity of >98%. The identity of the final product was verified by ESI-MS using a VG Quattro mass spectrometer (Micromass, Altricham, UK), equipped with standard electrospray ion source. Molecular weight calculations were performed by deconvolution using MassLynx^{TM} software version 2.00. The calculated weight of $G\alpha_s(350–394)$ was 5378 vs a molecular weight of 5377 found by mass spectrometry.

NMR Analysis

Samples for NMR analysis were prepared to obtain a 1 mM solution of the peptide and a 100 mM solution of SDS. To check the absence of an aggregation state of the polypeptide, spectra were recorded in the concentration range (0.05–15 mM). No significant changes were observed in the distribution or in the shape of the ^1H resonances, indicating that no aggregation phenomena occurred in this concentration range. After lyophilization of the sample prepared with the non-deuterated solvent, the residue consisting of $G\alpha_s(350–394)$ and SDS was dissolved in ^2H_2O and NOESY experiments were recorded after 5, 10 and 24 h to analyse the kinetic exchange.

One-dimensional (1D) NMR spectra were recorded in the Fourier mode with quadrature detection and the water signal was suppressed by a low-power selective irradiation in the homogated mode. DQF-COSY [19], TOCSY [20,21] and NOESY [22,23] experiments were run in the phase-sensitive mode using quadrature detection in $\omega1$ by time-proportional phase increase of the initial pulse. Data block sizes comprised 2048 addresses in t2 and 512 equidistant t1 values. Before Fourier transformation, the time domain data matrices were multiplied by shifted $\sin^2$ functions in both dimensions. A mixing time of 70 ms was used for the TOCSY experiments. NOESY experiments were run at 310 K with mixing times in the range 50–250 ms. The NOESY used for the structure calculation was recorded with a mixing time of 150 ms and did not display spin diffusion effects.

The chemical shift assignment of the $G\alpha_s(350–394)$ protons was achieved via the standard systematic application of DQF-COSY, TOCSY and NOESY experiments with the support of the SPARKY software [24].

NMR Diffusion Experiments

Self-diffusion coefficients were determined by the PFG NMR technique, using the stimulated echo method [25]. The $G\alpha_s(350–394)$ self-diffusion coefficient was determined by following the NMR signal (chemical shift 7.12 ppm), while for the SDS self-diffusion coefficient the decay of the overlapping signal of the methylene resonances (chemical shift 1.19 ppm) was analysed. The estimated uncertainty on the self-diffusion data is 5%.

Structure Calculations

Peak volumes were translated into upper distance bounds with the routine CALIBA of the DYANA software [26]. The necessary pseudoatom corrections were applied for non-stereospecifically assigned protons at prochiral centres and for the methyl groups. After discarding redundant and duplicated constraints, the final list included 410 constraints, which were used to generate an ensemble of 50 structures by the standard protocol of simulated annealing in torsion angle space implemented in DYANA. No dihedral angle restraints and no hydrogen bond restraints were applied. Molecular dynamics runs were performed using the SANDER module of the AMBER 5 software at a constant temperature of 300 K, using a nonbonded cutoff of 12 Å and a distance-dependent dielectric term ($e = 4 * r$) [27,28]. The molecular dynamics simulations were performed with a rather drastic limitation of allowed movements for the backbone atoms, whereas the side-chain atoms were allowed to move according to a small value of force constant restraints. A force constant of 1000 kcal/mol Å was applied on the NOE derived distance restraints of the backbone atoms, whereas a force constant of 10 kcal/mol Å was used to constrain the side-chain atoms. After 1 ps of heating and 10 ps of initialization time, the system was subjected to a 500 ps simulation with 1 fs time steps. Structures were saved every 5 ps. The final structures were analysed using the Insight 2000 program (Accelrys, San Diego, CA) [29].

RESULTS AND DISCUSSION

The study of the solution conformational properties of peptides involves an initial step that is the choice of an appropriate solvent medium. Water is known to be the most significant biological medium in which to perform structural studies. However, in NMR spectroscopy water solutions are affected by technical problems linked both to the solubility properties of the peptides and to the ability of water to increase peptide flexibility that hampers the observation of any possible ordered conformation. In principle $G\alpha_s(350–394)$ could have the right dimension to elicit a well defined secondary structure in water. So a full NMR investigation was undertaken in water solution. However, $G\alpha_s(350–394)$ is characterized by poor solubility in the physiological

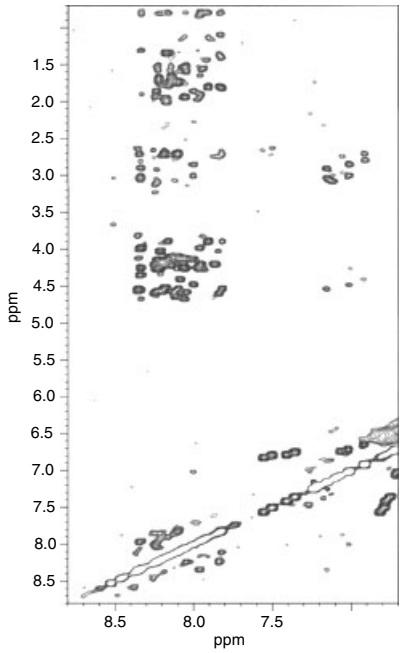

Figure 1 Amide region of the NOESY spectra of $G\alpha_s(350–394)$ in $H_2O/^2H_2O$ 90/10 v : v (mixing time 150 ms, 310 K).

pH range, so that TOCSY and NOESY experiments were recorded in water at pH = 5.0. Unfortunately, a detailed analysis of the spectra in water was hampered by the bad quality of the NMR spectra that are characterized by numerous overlapped signals and appear to be devoid of diagnostic NOE effects (Figure 1).

The assumption that water is the most biocompatible medium does not consider the fact that many biological environments are well represented as interface conditions between different compartments which cannot be properly represented by solutions of water alone. Under these conditions the exploration of new biologically significant media is advisable. Due to the ability of the *C*-terminus $G\alpha_s$ subunit to interact with membrane receptors, the exploration of the conformational properties of $G\alpha_s(350–394)$ in a membrane mimicking environment is biologically significant [30,31]. The membrane environment is usually mimicked by surfactant supramolecular aggregates, generally constituted by an apolar inner core and an hydrophilic exposed interface.

Although a variety of surfactant supramolecular structures have been proposed, in the NMR field the choice is limited due to the high costs of the surfactant deuteration and the usually low quality of the spectra produced in such systems. Micellar solutions of SDS, DPC, DPPC, are typically employed for NMR investigations [17]. At a concentration higher than the critical micellar (8 mM at 298 K) SDS molecules form spherical micelles with a mean aggregation number of ~58 and a diameter of ~40 Å [32,33]. Despite the fact that DPC and DPPC are considered to be more

membrane mimetic, SDS is often preferred because of the better quality of the NMR spectra.

In the present work a whole set of 1D and 2D ^1H homonuclear spectra was recorded on Gα_s(350–394) in a SDS micelle solution. Both the polypeptide molecular conformation and the structure of the surfactant/polypeptide aggregates have been analysed.

$H_2O/^2H_2O$ Exchange Kinetics

In the NMR analysis of proteins, the data deriving from $H_2O/^2H_2O$ exchange experiments give information on the implication of each amide NH group in hydrogen bonds and on their exposure to the solvent. Thus, the regions belonging to the core of the macromolecule can be distinguished from those more exposed to the environmental medium [34]. In a SDS micelle solution, $H_2O/^2H_2O$ exchange experiments have been demonstrated to be a useful tool to explore the location of the peptide relative to the SDS micelles [35,36]. Furthermore, the ^2H_2O NMR analysis of a large and unlabelled biomolecule enhances the information that can be obtained from homonuclear spectra which, due to the high number and the broadness of the signals, are very crowded.

Thus, an NMR investigation of Gα_s(350–394) in SDS/^2H_2O solution was performed to facilitate the analysis of the 2D spectra. The observation of the exchange kinetics of the amide protons was aimed at obtaining information on the interactions between the molecule and the micelles. 1D proton spectra were recorded 5 and 10 min after dissolution of Gα_s(350–394) in ^2H_2O/SDS solution, while 2D NOESY experiments were recorded in the time range of 5, 10 and 24 h. Figure 2 shows a comparison of the amide regions of the 2D NOESY spectra of Gα_s(350–394) recorded, respectively, in SDS/H_2O (Figure 2a), and at 5 and 24 h (respectively, Figure 2b and Figure 2c) after dissolution in the ^2H_2O/SDS solution. Surprisingly, the NOESY spectra of Gα_s(350–394) recorded 24 h after ^2H_2O dissolution still exhibit several correlations deriving from non-exchanged NH signals.

In the protein NMR spectra the NHs characterized by a slow exchange rate are typical of β-strand residues interacting with each other through hydrogen bonds. This finding means that long-range NOEs, derived from correlations of protons of spin systems not neighbours in the sequence, are observable. On the contrary, in the NOESY spectra of Gα_s(350–394) the signals that survived the ^2H_2O exchange showed many sequential correlations. The NOESY spectrum of Gα_s(350–394) obtained 5 h after ^2H_2O/SDS dissolution showed correlations relative to a short segment inside Gα_s(350–394), involving residues 372–384. The chemical shifts and the NOE correlations of the protons belonging to this region are reported in Table 1 and in Figure 3a, respectively. These residues, defining a segment extending from Ile372 to Leu384, show a correlation pattern typical of the α-helical structure, as suggested by the presence of dNN(i, i + 1) and dαN(i, i + 1) sequential connectivities and several dαN(i, i + 3), d$\alpha\beta$(i, i + 3), dαN(i, i + 4) medium-range connectivities. These NOEs translated in interprotonic distances were the basis for the structure calculations

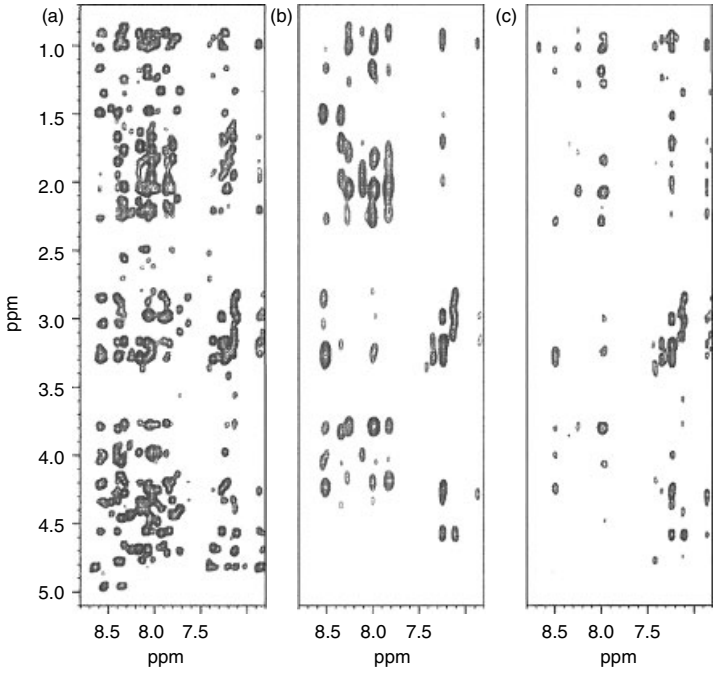

Figure 2 Amide regions of the NOESY spectra of Gα_s(350–394) in H_2O/SDS(a) and in ^2H_2O/SDS recorded 5 h (b) and 24 h (c) after dissolution of the peptide in the deuterated medium (600 MHz, 310 K, 1.8 mM).

Table 1 ^{1}H Chemical Shift Assignments for $G\alpha_s(350–394)$ (100 mM SDS, 600 MHz and 310 K). All Values Are Referred to the Water Residue Signal

Residue	NH	$C^{\alpha}H$	$C^{\beta}H$	$C^{\gamma}H$	$C^{\delta}H$	Other
Thr^{350}	7.94	4.14	4.02	1.04		
Ala^{351}	8.22	4.22	1.27			
Ser^{352}	8.03	4.25	3.72 3.70			
Gly^{353}	8.14	3.84				
		3.82				
Asp^{354}	8.15	4.58	2.75 2.73			
Gly^{355}	8.18	3.78				
		3.76				
Arg^{356}	7.77	4.06	1.55 1.41		3.01 2.99	Hε6.96
His^{357}	8.09	4.44	2.96 2.94			2H 8.44
						4H 7.06
Tyr^{358}	7.67	4.35	2.80 2.62			2,6H 6.92
						3,5H 6.64
Ala^{359}	7.71	4.16	1.14 1.12			
Tyr^{360}	7.50	4.51	2.90 2.74			2,6H 6.94
						3,5H 6.64
Pro^{361}		4.21	2.04 1.46	1.80 1.74	3.51 3.36	
His^{362}	8.01	4.48	3.06 3.04			2H 8.44
						4H 7.12
Phe^{363}	7.94	4.45	3.05 2.98			2,6H 7.17
						4H 7.11
Thr^{364}	7.84	4.04	4.09	1.03		
Ser^{365}	7.75	4.27	3.79 3.77			
Ala^{366}	7.82	4.20	1.28			
Val^{367}	7.52	3.93	1.92			
			0.76 0.75			
Asp^{368}	8.12	4.73	3.07 2.85			
Thr^{369}	8.23	3.81		1.15		
Glu^{370}	8.13	4.00	2.02 1.96	2.41 2.39		
Asn^{371}	8.28	4.14	2.75 2.67			$\gamma NH_2$7.586.86
Ile^{372}	7.65	3.56	1.82	1.54 1.02		
			0.81	0.71		
Arg^{373}	7.92	3.76	1.85 1.68		2.55 2.53	Hε7.03
Arg^{374}	7.69	3.97	1.85 1.62		3.19 3.17	Hε7.00
Val^{375}	7.81	3.57	2.07			
			0.98 0.82			
Phe^{376}	8.30	4.00	3.09 3.04			2,6H 7.05
Asn^{377}	8.35	4.13	2.83 2.65			$\gamma NH_2$7.416.88
Asp^{378}	8.23	4.33	3.08 3.06			
Ala^{379}	8.35	3.82	1.30			
Arg^{380}	8.17	3.61	1.76 1.52	1.41 1.39	2.99 2.97	Hε7.03
Asp^{381}	7.81	4.24	3.03 2.82			
Ile^{382}	7.80	3.56	1.84	1.22 1.20		
			0.80			
Ile^{383}	8.07	3.54	1.54	0.70		
			0.81			
Gln^{384}	8.10	3.94	2.07 1.98	2.51 2.32		7.16 6.59
Arg^{385}	7.83	4.03	1.65 1.47		3.20 3.18	Hε7.84
Met^{386}	7.93	4.12	2.03 1.86	2.60 2.42		
His^{387}	7.91	4.52	3.14 3.12			2H 8.48
						4H 7.20
Leu^{388}	8.07	4.05	1.63 1.48			0.81 0.79
Arg^{389}	7.63	3.97	1.63 1.47		3.05 3.03	Hε6.95

(*continued overleaf*)

Table 1 (*Continued*)

Residue	NH	$C^{\alpha}H$	$C^{\beta}H$	$C^{\gamma}H$	$C^{\delta}H$	Other
Gln^{390}	7.87	4.02	2.02 1.80	2.39 2.37		7.08 6.66
Tyr^{391}	7.63	4.35	2.97 2.78			2,6H 7.05
						3,5H 6.68
Glu^{392}	7.86	4.17	2.01 1.87	2.31 2.29		
Leu^{393}	7.91	4.12	1.53 1.43			0.83 0.77
Leu^{394}	7.59	4.23	1.62 1.49			0.83 0.70

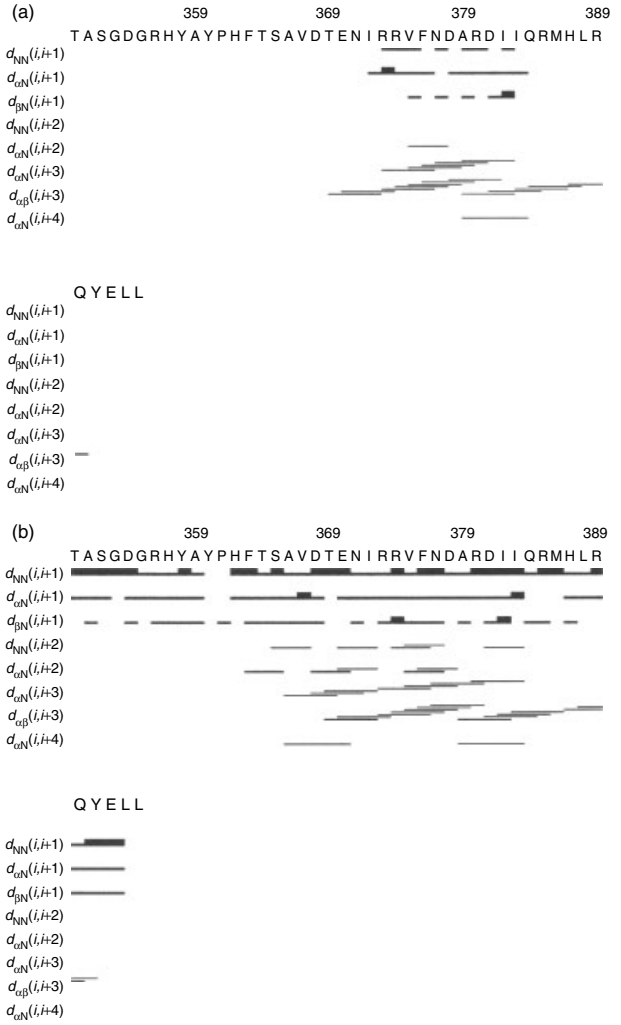

Figure 3 Sequential and medium-range NOEs for $G\alpha_s(350–394)$. Data were obtained from a 600 MHz NOESY experiment (mixing time 150 ms, 310 K) collected in (a) ^2H_2O/SDS (10 h after dissolution of the peptide) and (b) H_2O/SDS.

that were performed by simulated annealing procedures using as restraints 70 intraresidue, 54 short-range and 45 medium-range connectivities. The structures superimposed at level of the residues Ile372 – Leu384 show a rmsd of 0.8 Å. The PROCHECK analysis of the dihedral angles relative to this fragment is consistent with the presence of an α-helical structure [37]. The results of the $H_2O/^2H_2O$ exchange lead to the hypothesis of a large prevalence of the micelle-bound peptide molecules driven by a strong interaction of the region of $G\alpha_s(372–384)$ with the SDS micelles.

Chemical Shift Assignment and Structure Calculations

The 2D homonuclear TOCSY and NOESY experiments recorded in non deuterated water solution led to the chemical shift assignment of the whole $G\alpha_s(350–394)$ according to the Wüthrich procedure (Table 1) [38]. The observation of the signals that were not evident in ^2H_2O led to the collection of many additional short-and medium-range NOEs. These correlations allowed the determination of the full secondary structure arrangement of $G\alpha_s(350–394)$. Figure 3b reports the short- and medium-range NOEs relative to the whole molecule. The pattern of NOE connectivities is strongly suggestive of an α-helical structure encompassing the central and *C*-terminal residues of the biomolecule. The remaining portion extending towards the *N*-terminus shows only sequential NOEs, suggesting an unordered conformation.

Three-dimensional structures of $G\alpha_s(350–394)$ were calculated by restrained simulated annealing procedures based on 388 intraresidue, 157 short-range, 139 medium-range and 5 long-range NOEs (DYANA software package) [26]. The calculations followed the same procedure discussed in the previous section. Figure 4 reports the 20 best structures of $G\alpha_s(350–394)$ minimized with the SANDER module of the AMBER 5.0 package [27,28]. The models are overlapped at the level of Asp368 – Glu392 where the rmsds from the average are 0.76 Å (backbone heavy atoms) and 1.32 Å (all heavy atoms). In agreement with NOESY data, the structure bundle shows a helical structural arrangement spanning residues Ile372 – Glu392. The residues Tyr360–Asp368 show a higher flexibility, in particular a β-turn structure involves the segment Thr364–Asp368. Extended conformations characterize the Thr350–Tyr360 *N*-terminal residues.

Figure 5 shows a comparison between the $G\alpha_s(350–394)$ NMR structure and the corresponding region

Figure 4 The best 20 calculated structures of $G\alpha_s(350–394)$ as derived from DYANA calculations and energy minimized using the SANDER module of AMBER 5.0 software. The structures are overlapped at the level of the $Asp^{368}–Glu^{392}$ segment. The region coloured in green involves residues $Ile^{372}–Gln^{384}$ which show a significant resistance to the $H_2O/^2H_2O$ exchange.

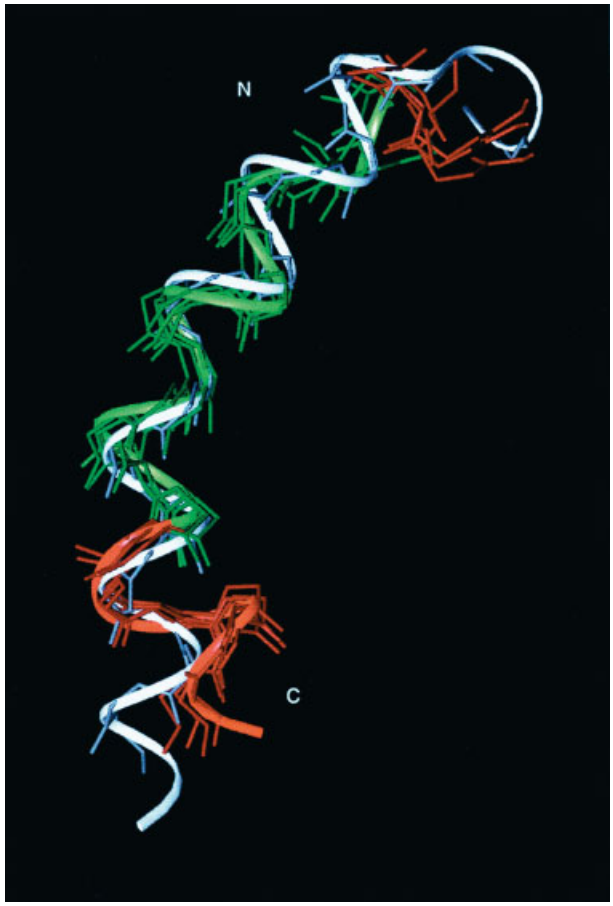

Figure 5 Ribbon representation of the 372–392 α-helix of $G\alpha_s(350–394)$ superimposed on the corresponding portion of the $G\alpha_s$ protein crystal structure (white ribbon). Green portion of the ribbon is relative to the 372–384 segment of $G\alpha_s(350–394)$, the remaining portion is coloured in red.

of the crystal structure of the $G\alpha_s$ protein (ref. code 1AZT) [6]. The long *C*-terminal helix found in the SDS micelle solution is in excellent agreement with the corresponding region of the protein that in the crystal structure is named α5 helix. The segment Ile372–Gln384 of $G\alpha_s(350–394)$ that was found in close interaction with the micelle structure corresponds to the beginning of the α5 helix. The $G\alpha_s(350–394)$ *C*-terminal helix keeps the same size of the α5 helical stretch found in the crystal structure.

A comparison of the $G\alpha_s(350–394)$ NMR structure in SDS with those of $G\alpha_s(384–394)$, $G\alpha_s(380–394)$, $G\alpha_s(374–394)$, previously solved [10–12], shows that the presence of additional residues up to the *N*-terminus gives stability to the *C*-terminal secondary structure. In the $G\alpha_s$ 45-mer fragment the *C*-terminal α-helix spans residues Ile372 – Glu392, whereas the longest segment of α-helical structure found in

Table 2 Self-Diffusion Coefficients of $G\alpha_s(350–394)$ and SDS in Heavy Water at 300 and 310 K. Hydrodynamic Radii of the $G\alpha_s(350–394)$–SDS Aggregates. Number of SDS Molecules Bound per $G\alpha_s(350–394)$ Molecule

T/K	[SDS]/M	[$G\alpha_s(374–394)$]/M	$D_s \times 10^9/m^2s^{-1}$	$D_p \times 10^9/m^2s^{-1}$	R_h/Å	n_s
300	0.1528	—	0.0512	—	—	
300	0.1528	0.0015	0.0202	0.0114	175	78
300	0.1018	0.0010	0.0226	0.0178	112	86
310	0.1528	—	0.0552			
310	0.1528	0.0015	0.0260	0.0185	133	80
310	0.1018	0.0010	0.0291	0.0202	121	74

$G\alpha_s(374–394)$ [12] involves the residues 380–394. Thus, the increased residue number of the peptide and the membrane mimetic environment seem to play a stabilizing role. As a consequence, the residues that in $G\alpha_s(374–394)$ were found in a random coil conformation, in $G\alpha_s(350–394)$ are well structured and belong to the helical fragment in close contact with the micelles.

NMR Diffusion Experiments

The self-diffusion coefficients of proteins and peptides are useful tools for obtaining structural information [39], as diffusion is closely related to the hydrodynamic radius of the particles involved.

Pulsed-field gradient NMR experiments [40] were performed on the $G\alpha_s(350–394)$ sample in SDS micellar solution at both 300 and 310 K. The self-diffusion coefficients of the polypeptide $G\alpha_s(350–394)$, D_p, and that of the surfactant SDS, D_s, are shown in Table 2. For comparison, measurements were also performed in a SDS–water binary mixture at the same SDS concentration employed to solubilize the polypeptide. In all samples, both at 300 K and at 310 K, D_s in the presence of $G\alpha_s(350–394)$ is lower than that measured in the absence of the peptide. As inferred from $H_2O/^2H_2O$ exchange experiments, a largely prevalent fraction of $G\alpha_s(350–394)$ molecules interact with SDS, forming $G\alpha_s(350–394)$–SDS aggregates, so that it is reasonable to assume that D_p coincides with the self-diffusion coefficient of the aggregates. Accordingly, D_p can be related to the aggregate hydrodynamic radius, R_h, through the Stokes-Einstein equation [41]. The estimated R_h values are shown in Table 2. It is interesting to note that the R_h values are significantly higher than those reasonably expected for a single polypeptide solubilized in a SDS micelle.

A qualitative estimation of the number of SDS molecules per polypeptide chain in the aggregate can be obtained by considering that the SDS molecules are present in the $G\alpha_s(350–394)$-containing solution in three different aggregation states: free monomers, micelles and $G\alpha_s(350–394)$–SDS aggregates. Consequently, its self-diffusion coefficient is an average value according to the relation:

$$D_s = p_s^{mon} D_s^{mon} + p_s^{mic} D_s^{mic} + p_s^{agg} D_s^{agg} \qquad (1)$$

where D_s^{mon}, D_s^{mic} and D_s^{agg} are the self-diffusion coefficients of SDS molecules as monomers, micelles and $G\alpha_s(350–394)$–SDS aggregates, respectively; p_s^{mon}, p_s^{mic} and p_s^{agg} are the fractions of SDS molecules in the different states. As the SDS concentration is much higher than the cmc, the contribution of free monomers can be neglected. The self-diffusion coefficient of SDS micelles, D_s^{mic}, can be evaluated from measurements in the absence of $G\alpha_s(350–394)$. Furthermore, the SDS molecules taking part in the aggregates with $G\alpha_s(350–394)$ should move together with the polypeptide, i.e. $D_s^{agg} = D_p$. In all these assumptions, p_s^{agg} can be estimated from equation (1), allowing, in turn, the estimation of the average number of SDS molecules bound to each $G\alpha_s(350–394)$ molecule, n_s. Inspection of Table 2 shows that n_s is higher than the surfactant aggregation number and is almost unaffected by the solute concentration and by the temperature.

To summarize, all the NMR diffusion data suggest the formation of an aggregate constituted by several polypeptide chains and ~80 SDS molecules per polypeptide.

A Model for the $G\alpha_s(350–394)$ Interaction with Anionic Surfactants

The data relative to the self-diffusion coefficients and the H/D exchange kinetics provide important clues for understanding the behaviour of the polypeptide at the interface. Concerning the H/D exchange kinetics, $G\alpha_s(350–394)$ dissolved in SDS micellar solution shows a significant resistance of the backbone proton in the region 372–384 to H/D exchange. This segment includes four positively charged Arg residues. The analysis of the side-chain conformational space of segment 372–384 shows a common orientation of the Arg373 and Arg380 residues, that define a positively charged surface (Figure 6). Thus, it is reasonable to suppose an interaction of this side of the region 372–384 with the negatively charged surface of the micelle. Furthermore, the number of hydrophobic residues in the portion 372–384, together with its low water solubility, which is strongly enhanced in the presence of the SDS micelles, suggests an hydrophobic

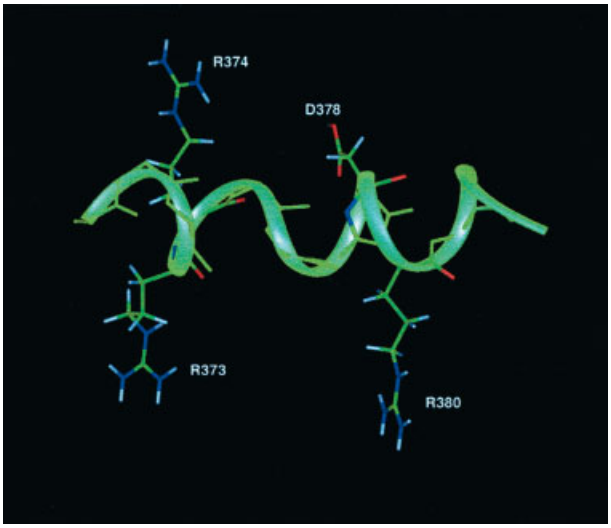

Figure 6 Ribbon representation of the Ile^{372}–$Gln^{384}G\alpha_s$ (350–394) fragment. The side chains of Arg^{372}, Arg^{373}, Asp^{378} and Arg^{380} are displayed and coloured by atom type.

interaction taking place between these residues and the inner core of the surfactant aggregate.

An analysis of the self-diffusion coefficients can give some insights into the aggregation process through which surfactant micelles solubilize biomolecules. Indeed, in the case of large molecules, such as long polypeptides, the guest molecule can act as a nucleation site for surfactant self-aggregation, leading to supramolecular structures the size and dimension of which is tailored to accommodate the guest molecule or large segments of it.

Concerning our system, the self-diffusion data indicate that the number of the SDS molecules interacting with a single molecule of $G\alpha_s(350–394)$ is higher than the typical surfactant aggregation number, suggesting that the surfactant self-aggregation process is enhanced in the presence of the polypeptide. Furthermore, the values of the hydrodynamic radius support the hypothesis of the formation of a supramolecular structure containing several $G\alpha_s(350–394)$ chains which, however, do not interact with each other, as evident from NMR mono-dimensional experiments recorded at several different peptide concentrations (vide infra). The large dimensions of the $G\alpha_s(350–394)$ aggregates can somehow explain the resistance of the backbone protons of segment 372–384 to the H/D exchange. Indeed, the big super-aggregate allows the region 372–384 to be preserved from the solvent access for a significantly long time.

The alignment of the sequences of the *C*-terminal regions of $G\alpha_s$ proteins highlights the presence of many highly conserved residues of Val375, Phe376, Asp378, Asp381, Ile383, Leu388 and Leu393. It is relevant to note that many of these residues belong to the previous discussed fragment $G\alpha_s(372–384)$.

According to a general model of receptor/G protein coupling, interactions occurring between highly conserved residues of both G protein and its cognate receptors [42] play a decisive role in generating contacts critical for receptor/G protein interaction [43–47]. In particular, a dipolar interaction between two Asp residues in helix α5 of the Gα subunit and the Arg residue in the DRY motif (conserved in 99% of receptors) of the transmembrane domain III of the receptor could generate the conformational transition that drives the whole coupling process.

The data concerning the interaction between the region 372–384 and the micellar surface prompt interesting speculations regarding the role of the perimembrane environment in promoting the receptor/G protein interaction. The significant stabilization exerted by the interface compartment on the *N*-terminus of the α5-helix allows one to speculate that the contact with the membrane compartment can be a way to stabilize the *C*-terminal helix. Indeed, as previously discussed, residues essential for the coupling process are located in this segment. In particular, the definition of the polar face of the helix exposing the Arg373 and Arg380 residues has the further important consequence of limiting the conformational freedom of Asp378 through an electrostatic interaction with Arg374 oriented on the opposite face of the helix (Figure 6). Last but not least, according to the hypothesis that a key transition in the G protein/receptor interaction takes place through the region between the α4/α5 helices [13–16], the beginning of the α5 helix could play the role of a structurally highly stable segment able to transfer the conformational perturbation to the last undecapeptide α-helical segment.

CONCLUSIONS

$G\alpha_s(350–394)$, the 45-mer polypeptide corresponding to the *C*-terminal region of the $G\alpha_s$ subunit, was structurally investigated by NMR spectroscopy in a SDS micellar environment. The interface compartment defined by the SDS micellar solutions seems to play a relevant role in the stabilization of the secondary structure of the $G\alpha_s$ *C*-terminus. The structural arrangement of the examined region is in good agreement with that known through the crystal coordinates of the $G\alpha_s$ protein. The data relative to the $H_2O/^2H_2O$ exchange experiments, as well as those relative to the NMR diffusion experiments, show that the peptide interacts strictly with the micellar compartment defining an aggregate of unusual dimensions. The interaction of the macromolecule with the micelle compartment is fundamental to preserving the side-chain orientation of several residues considered crucial for the receptor interaction.

REFERENCES

1. Hamm HE. The many faces of G protein signals. *J. Biol. Chem.* 1998; **273**: 669–672.
2. Noel J, Hamm HE, Sigler PB. The 2.2 Å crystal structure of transducin-α complexed with GTPγs. *Nature* 1993; **366**: 654–663.
3. Lambright DG, Noel JP, Hamm HE. Structural determinants for the activation of the α-subunit of a heterotrimeric G protein. *Nature* 1994; **369**: 621–628.
4. Coleman DE, Berghuis AM, Lee E, Linder ME, Gilman GA, Sprang SR. Structure of active conformations of $G_{i\alpha1}$ and the mechanism of GTP hydrolysis. *Science* 1994; **265**: 1405–1412.
5. Mixon MB, Lee E, Coleman DE, Berghuis AM, Gilman AG, Sprang SR. Tertiary and quaternary structural changes in $G_{i\alpha1}$ induced by GTP hydrolysis. *Science* 1995; **270**: 954–960.
6. Sunahara RK, Tesmer JJG, Gilman AG, Sprang SR. Crystal structure of the adenylyl cyclase activator $G_{s\alpha}$. *Science* 1997; **278**: 1943–1947.
7. Dratz EA, Gizachew D, Busse SC, Rens-Domiano S, Hamm HE. NMR structure of a receptor bound G-protein peptide: structure refinement and update. *Biophys. J.* 1996; **70**: A16.
8. Kisselev OG, Kao J, Ponder JW, Fann YC, Gautam N, Marshall GR. Light-activated rhodopsin induces structural binding motif in G protein α subunit. *Proc. Natl Acad. Sci. USA* 1998; **95**: 4270–4275.

9. Koenig BW, Kontaxis G, Mitchell DC, Louis JM, Litman BJ, Bax A. Structure and orientation of a G protein fragment in the receptor bound state from residual dipolar couplings. *J. Mol. Biol.* 2002; **322**: 441–461.
10. Mazzoni MR, Taddei S, Giusti L, Rovero P, Galoppini C, D'Ursi AM, Albrizio S, Triolo A, Novellino E, Greco G, Lucacchini A, Hamm HE. A Ga_s carboxyl-terminal peptide prevents G_s activation by the A_{2A} adenosine receptor. *Mol. Pharmacol.* 2000; **58**: 226–236.
11. Albrizio S, D'Ursi AM, Fattorusso C, Galoppini C, Greco G, Mazzoni MR, Novellino E, Rovero P. Conformational studies on a synthetic *C*-terminal fragment of the α subunit of G_s proteins. *Biopolymers* 2000; **54**: 186–194.
12. D'Ursi AM, Albrizio S, Greco G, Mazzeo S, Mazzoni MR, Novellino E, Rovero P. Conformational analysis of the *C*-terminal 15-residue fragment of the $G\alpha_s$ protein. *J. Pept. Sci.* 2002; **8**: 476–488.
13. Natochin M, Moussaif M, Artemyev NO. Probing the mechanism of rhodopsin-catalyzed transducin activation. *J. Neurochem.* 2001; **77**: 202–210.
14. Blahos J, Fisher T, Brabet I, Stauffer D, Rovelli G, Bockaert J, Pin JP. A novel site on the $G\alpha$-protein that recognizes heptahelical receptors. *J. Biol. Chem.* 2001; **276**: 3262–3269.
15. Bockaert J, Pin JP. Molecular tinkering of G protein-coupled receptors: an evolutionary success. *EMBO J.* 1999; **18**: 1723–1729.
16. Mazzoni MR, Hamm HE. Interaction of transducin with light – activated rhodopsin protects it from proteolytic digestion by trypsin. *J. Biol. Chem.* 1996; **271**: 30 034–30 040.
17. Bader R, Lerch M, Zerbe O. NMR of membrane-associated peptides and proteins. Methods and principles in medicinal chemistry. *BioNMR Drug Res.* 2003; **16**: 95–120.
18. Grieco P, Albrizio S, D'Ursi AM, Giusti L, Mazzoni MR, Novellino E, Rovero P. A structure – activity relationship study on position −2 of the $G\alpha_s$ *C*-terminal peptide able to inhibit Gs activation by A_{2A} adenosine receptor. *Eur. J. Med. Chem.* 2003; **38**: 13–18.
19. Piantini U, Sorensen OW, Ernst RR. Multiple quantum filters for elucidating NMR coupling network. *J. Am. Chem. Soc.* 1982; **104**: 6800–6801.
20. Braunschweiler L, Ernst RR. Coherence transfer by isotropic mixing: application to proton correlation spectroscopy. *J. Magn. Reson.* 1983; **53**: 521–528.
21. Bax A, Davis DG. Practical aspect of two-dimensional transverse NOE spectroscopy. *J. Magn. Reson.* 1985; **63**: 207–213.
22. Macura S, Ernst RR. Elucidation of cross relaxation in liquids by two-dimensional NMR spectroscopy. *Mol. Phys.* 1980; **41**: 95–117.
23. Jeener J, Meyer BH, Bachman P, Ernst RR. Investigation of exchange processes by two-dimensional NMR spectroscopy. *J. Chem. Phys.* 1979; **71**: 4546–4553.
24. Goddard TD, Kneller DG. *Sparky 3*. University of California: San Francisco.
25. Stejskal EO, Tanner JE. Spin diffusion measurements: spin echoes in the presence of a time-dependent field gradient. *J. Phys. Chem.* 1965; **42**: 288–292.
26. Güntert P, Mumenthaler C, Wüthrich K. Torsion angle dynamics for NMR structure calculation with the new program DYANA. *J. Mol. Biol.* 1997; **273**: 283–298.
27. Case DA, Pearlman DA, Caldwell JW, Cheatham III TE, Ross WS, Simmerling CL, Darden TA, Merz KM, Stanton RV, Cheng AL, Vincent JJ, Crowley M, Ferguson DM, Radmer RJ, Seibel GL, Singh UC, Weiner PK, Kollman PA. *AMBER 5*, 1997; University of California: San Francisco.
28. Pearlman DA, Case DA, Caldwell JW, Ross WS, Cheatham III TE, DeBolt S, Ferguson D, Seibel G, Kollman P. AMBER, a package of computer programs for applying molecular mechanics, normal mode analysis, molecular dynamics and free energy calculations to simulate the structural and energetic properties of molecules. *Comput. Phys. Commun.* 1995; **91**: 1–41.
29. Accelrys, 2001; San Diego, CA.
30. Moroder L, Romanio R, Guba W, Mierke DF, Kessler H, Delporte C, Winand J, Christophe J. New evidence for a membrane-bound pathway in hormone receptor binding. *Biochemistry* 1993; **32**: 13 551–13 559.
31. Schwyzer R. Peptide-membrane interactions and a new principle in quantitative structure-activity relationships. *Biopolymers* 1991; **31**: 785–792.
32. Fennell ED, Mukherjee S, Mitchell DJ, Ninham BW. Surfactant diffusion: new results and interpretation. *J. Colloid. Interface Sci.* 1983; **93**: 184–204.
33. Nilsson PG, Lindman B. Mixed micelles of nonionic and ionic surfactants. A nuclear magnetic resonance self-diffusion and proton relaxation study. *J. Phys. Chem.* 1984; **88**: 5391–5397.
34. Shao H, Jao S, Ma K, Zagorski MG. Solution structures of micelle-bound amyloid β-(1–40) and β-(1–42) peptides of Alzheimer's disease. *J. Mol. Biol.* 1999; **285**: 755–773.
35. Spyracopoulos L, O'Neil JDJ. Effect of a hydrophobic environment on the hydrogen exchange kinetics of model amides determined by ^{1}H-NMR spectroscopy. *J. Am. Chem. Soc.* 1994; **116**: 1395–1402.
36. Yee A, Szymczyna B, O'Neil JDJ. Backbone dynamics of detergent-solubilized alamethicin from amide hydrogen exchange measurements. *Biochemistry* 1999; **38**: 6489–6498.
37. Laskowski RA, MacArthur MW, Moss DS, Thornton JM. PROCHECK: a program to check the stereochemical quality of protein structures. *J. Appl. Crystallogr.* 1993; **26**: 283–291.
38. Wüthrich K. *NMR of Proteins and Nucleic Acids*. Wiley: New York, 1986.
39. Gao X, Wong TC. Studies of the binding and structure of adrenocorticotropin peptides in membrane mimics by NMR spectroscopy and pulsed-field gradient diffusion. *Biophys. J.* 1998; **74**: 1871–1888.
40. Stilbs P. Fourier transform pulsed-gradient spin-echo studies of molecular diffusion. *Progr. NMR Spectrosc.* 1987; **19**: 1–45.
41. Robinson RA, Stokes RH. *Electrolyte Solutions*. Butterworths: London, 1955.
42. Oliveira LA, Paiva CM, Vriend G. A low resolution model for the interaction of G proteins with G protein-coupled receptors. *Protein Eng.* 1999; **12**: 1087–1095.
43. Conklin BR, Farfel Z, Lustig KD, Julius D, Bourne HR. Substitution of three amino acids switches receptor specificity of $G_q\alpha$ to that of $G_i\alpha$. *Nature* 1993; **363**: 274–276.
44. Kostenis E, Conklin BR, Wess J. Molecular basis of receptor/G protein coupling selectivity studied by coexpression of wild type and mutant m2 muscarinic receptors with mutant $G\alpha_q$ subunits. *Biochemistry* 1997; **36**: 1487–1495.
45. Kostenis E, Zeng F, Wess J. Functional characterization of a series of mutant G protein α_q subunits displaying promiscuous receptor coupling properties. *J. Biol. Chem.* 1998; **273**: 17 886–17 892.
46. Grishina G, Berlot CH. A surface-exposed region of $G_{s\alpha}$ in which substitutions decrease receptor-mediated activation and increase receptor affinity. *Mol. Pharmacol.* 2002; **57**: 1081–1092.
47. Bae H, Cabrera-Vera TM, Depree KM, Graber SG, Hamm HE. Two amino acids within the α4 helix of $G\alpha_{il}$ mediate coupling with 5-hydroxytryptamine$_{1b}$ receptors. *J. Biol. Chem.* 1999; **274**: 14 963–14 971.

